Strong Ferromagnetic Exchange Coupling and Single-Molecule Magnetism in MoS_4^{3-}-Bridged Dilanthanide Complexes

Lucy E. Darago,[a‡] Monica D. Boshart,[b‡] Brian D. Nguyen,[b] Eva Perlt,[b] Joseph W. Ziller,[b] Wayne Lukens,[c] Filipp Furche,[b] William J. Evans,[b]* and Jeffrey R. Long[a,d,e]*

[a]Department of Chemistry, University of California, Berkeley, California 94720, United States
[b]Department of Chemistry, University of California, Irvine, California 94697, United States
[c]Chemical Sciences Division, Lawrence Berkeley National Laboratory, Berkeley, California 94720, United States
[d]Department of Chemical and Biomolecular Engineering, University of California, Berkeley, California 94720, United States
[e]Materials Sciences Division, Lawrence Berkeley National Laboratory, Berkeley, California 94720, United States

ABSTRACT: We report the synthesis and characterization of the trinuclear 4d-4f compounds $[Co(C_5Me_5)_2][(C_5Me_5)_2Ln(\mu\text{-}S)_2Mo(\mu\text{-}S)_2Ln(C_5Me_5)_2]$, **1-Ln** (Ln = Y, Gd, Tb, Dy), containing the highly polarizable MoS_4^{3-} bridging unit. UV-Vis-NIR diffuse reflectance spectra and DFT calculations of **1-Ln** reveal a low-energy metal-to-metal charge transition assigned to charge transfer from the singly-occupied $4d_{z^2}$ orbital of Mo^V to the empty $5d_{z^2}$ orbital(s) of the lanthanide ($4d_{z^2}$ in the case of **1-Y**), mediated by sulfur-based 3p orbitals. Electron paramagnetic resonance spectra collected for **1-Y** in a tetrahydrofuran solution show large ^{89}Y hyperfine coupling constants of $A_\perp$ = 23 MHz, and $A_{||}$ = 26 MHz, indicating the presence of significant yttrium-localized unpaired electron density. Magnetic susceptibility data support similar electron delocalization and ferromagnetic Ln–Mo exchange for **1-Gd**, **1-Tb**, and **1-Dy**. This ferromagnetic exchange gives rise to an S = 15/2 ground state for **1-Gd** and one of the largest magnetic exchange constants involving Gd^{III} observed to date, with J_{Gd_Mo} = +16.1(2) cm^{-1}. Additional characterization of **1-Tb** and **1-Dy** by ac magnetic susceptibility measurements reveals that both compounds exhibit slow magnetic relaxation. For **1-Dy**, the extracted thermal relaxation barrier of U_{eff} = 68 cm^{-1} is the largest yet reported for a complex containing a paramagnetic 4d metal center. Together, these results provide a potentially generalizable route to enhanced *n*d-4f magnetic exchange, revealing opportunities for the design of new *n*d-4f single-molecule magnets and bulk magnetic materials.

INTRODUCTION

Single-molecule magnets, molecules that exhibit a well-isolated bistable magnetic ground state with a thermal barrier to relaxation of the magnetization, *U*, are of potential utility in applications such as high-density information storage and quantum information processing.[1] However, to date even the most promising systems are hindered by low operating temperatures, with upper limits defined by the blocking temperature, T_b, of a given molecule. Below this temperature, the magnetization remains pinned along the molecular magnetic easy axis and is not susceptible to thermal fluctuations, akin to the magnetic polarization within bulk magnetic materials. One particularly successful strategy for generating single-molecule magnets with high blocking temperatures has been to design systems exhibiting strong magnetic exchange interactions between highly anisotropic lanthanide ions, as exemplified by the diterbium(III) complex $\{[((Me_3Si)_2N)_2Ln(THF)]_2(\mu\text{-}N_2^{\bullet})\}^{1-}$.[2] Here, the diffuse spin orbital of the N_2^{3-} radical bridge is able to penetrate the core 4f magnetic orbitals to engender strong lanthanide-radical coupling, resulting in a highly anisotropic molecular species with a 100-s magnetic blocking temperature of 14 K, one of the highest known values for an exchange-coupled system. A blocking temperature of 20 K was subsequently observed for the related N_2^{3-}-bridged complex, $\{[(C_5Me_4H)_2Tb]_2(\mu\text{-}N_2^{\bullet})\}^{1-}$,[3] and in this and other exchange-coupled complexes the barrier to magnetic relaxation, which tracks to some extent with T_b, has been shown to be a function of the magnitude of the magnetic exchange coupling.[3,4] While recent efforts to enhance crystal field splitting and axiality of magnetic excited states in single-ion lanthanide magnets has led to outstanding advances in 100-s magnetic blocking temperatures, up to 65 K,[5] the combination of large magnetic anisotropy and large total angular momentum achieved via strong exchange between lanthanides remains a promising route to still higher blocking temperatures.

Radical-bridged lanthanide complexes offer the advantage of ligands with spin-carrying atoms directly coordinated to the lanthanide ion and therefore close enough to engage in direct exchange with the lanthanide spin density. In contrast, magnetic interactions between

lanthanides and other metal ions typically proceed via superexchange pathways across ligand atoms. As such, while lanthanide-transition metal pairings offer additional synthetic handles with which to design exchange-coupled single-molecule magnets, *n*d-4f single-molecule magnets typically exhibit very weak magnetic coupling, in most cases less than 5 cm^{-1}.[6] This weak coupling in turn leads to slow magnetic relaxation that is single-ion in origin or prompts low-lying exchange-coupled excited states that preclude large relaxation barriers.[4,6,9b,9c]

The heavier 4d and 5d transition metals have the potential to facilitate strong superexchange with lanthanides since their more diffuse d orbitals are more likely to have enhanced overlap with ligand orbitals.[7] Furthermore, there is better energy matching of 4d/5d spin-containing orbitals with the spin-carrying 4f and empty 5d lanthanide orbitals, as compared to 3d transition metals. Nearly all lanthanide coordination compounds that incorporate 4d and 5d paramagnetic metal ions (M) utilize cyano-ligated building units,[8] and all[8,9] of these compounds have yet to yield M–Gd coupling magnitudes of greater than 1.6 cm^{-1}.[8c,8i]

Considering candidate 4d bridging moieties with the potential for enhanced exchange strength, we turned to the MoS_4^{y-} (y = 2, 3) unit. The range of oxidation states available to molybdenum and the polarizability of the single-atom sulfide bridges render this moiety a promising ligand to facilitate strong magnetic communication. Herein, we report the synthesis and characterization of the MoS_4^{3-}-bridged complex salts $[Co(C_5Me_5)_2][(C_5Me_5)_2Ln(\mu\text{-}S)_2Mo(\mu\text{-}S)_2Ln(C_5Me_5)_2]$ (Ln = Y, Gd, Tb, Dy), **1-Ln**, accessed via one-electron reduction of the neutral Mo^{VI}-bridged complexes $(C_5Me_5)_2Ln(\mu\text{-}S)_2Mo(\mu\text{-}S)_2Ln(C_5Me_5)_2$. Static magnetic susceptibility measurements reveal strong 4f/5d-4d ferromagnetic exchange coupling in **1-Gd**, **1-Tb**, and **1-Dy**, which is proposed to occur via charge transfer from Mo^{V} to Ln^{III}, as supported by electron paramagnetic resonance and UV-Vis-NIR spectroscopies. Moreover, slow magnetic relaxation is observed for **1-Tb** and **1-Dy**.

EXPERIMENTAL

General Information. All manipulations and syntheses described were conducted with rigorous exclusion of air and water using standard Schlenk line and glovebox techniques under an argon or nitrogen atmosphere. Solvents were sparged with UHP argon (Praxair) and dried by passage through columns containing Q-5 and molecular sieves prior to use. NMR solvents (Cambridge Isotope Laboratories) were dried over NaK alloy, degassed by three freeze-pump-thaw cycles, and vacuum transferred before use. Reagents $Co(C_5Me_5)_2$ (Aldrich) and $(NH_4)_2MS_4$ (M = Mo, W; Aldrich), were used as received. The lanthanide trichlorides $LnCl_3$ (Ln = Y, Gd, Tb, Dy) were dried according to literature procedures by heating a mixture of the hydrated trichloride with an excess of NH_4Cl.[10] Potassium bis(trimethylsilylamide) ($K[N(SiMe_3)_2]$, Aldrich, 95%) was purified via toluene extraction before use. Pentamethylcyclopentadiene, (C_5Me_5H, Aldrich, 95%) was dried over molecular sieves and degassed using three freeze-pump-thaw cycles before deprotonation with $K[N(SiMe_3)_2]$ to form the ligand KC_5Me_5.[11] The precursor compounds $(C_5Me_5)_2Y(C_3H_5)$,[12] $(C_5Me_5)_2Ln(\mu\text{-}Ph)_2BPh_2$[13] (Ln = Y, Gd, Tb, Dy), and $(PPh_4)_2MoS_4$[14] were prepared using literature procedures. Proton NMR spectra were recorded on Bruker GN500 or CRYO500 MHz spectrometers ($^{13}C\{^1H\}$ at 125 MHz) at 298 K, unless otherwise stated, and referenced internally to residual protio-solvent resonances. Samples for IR spectroscopic analysis were prepared as KBr pellets and spectra were obtained on a Jasco FT/IR-4700 or Varian 1000 spectrometer. EPR spectra were collected using an X-band frequency (9.3–9.8 GHz) on a Bruker EMX Spectrometer equipped with an ER041XG microwave bridge, and the magnetic field was calibrated with 2,2-diphenyl-1-picrylhydrazyl (DPPH) (g = 2.0036). UV-visible-NIR diffuse reflectance spectra were collected using a CARY 5000 spectrophotometer interfaced with Varian Win UV software. The samples were held in a Praying Mantis air-free diffuse reflectance cell. Barium sulfate powder was used as a non-adsorbing matrix. The Kubelka-Munk conversion (F(R) vs. wavenumber) of the raw diffuse reflectance spectrum (R vs. wavenumber) was obtained by applying the formula F(R) = (1 − R)2/2R. Elemental analyses were conducted on a Perkin-Elmer 2400 Series II CHNS elemental analyzer.

$(C_5Me_5)_2Y(\mu\text{-}S)_2Mo(\mu\text{-}S)_2Y(C_5Me_5)_2$. A slurry of $(PPh_4)_2MoS_4$ (0.043 g, 0.048 mmol) in 3 mL of THF was added to a solution of $(C_5Me_5)_2Y(\mu\text{-}Ph)_2BPh_2$ (0.066 g, 0.097 mmol) in 2 mL of THF. The solution immediately became dark brown/purple and cloudy. After stirring for 1 h, the mixture was centrifuged to produce a purple supernatant and dark grey insoluble material. The supernatant was collected by filtration and the THF solvent was removed under reduced pressure to yield a dark brown/purple solid. The brown/purple solid was dissolved in toluene (5 mL) and cooled for 24 h at −35 °C to yield dark purple crystals (0.018 g, 43%) suitable for single-crystal X-ray diffraction, which enabled identification of the compound as Mo^{VI}-bridged $(C_5Me_5)_2Y(\mu\text{-}S)_2Mo(\mu\text{-}S)_2Y(C_5Me_5)_2$. ^1H NMR (C_6D_6): δ 2.09 (s, $C_5\mathit{Me_5}$, 60H). $^{13}C\{^1H\}$ NMR 128.4 (C_5Me_5), 12.2 ($C_5\mathit{Me_5}$). IR (cm^{-1}): 2960m, 2900s, 2850s, 2720w, 1960w, 1440m, 1380m, 1020m, 800w, 730m, 700w, 490s. Anal Calcd for $C_{40}H_{60}S_4Y_2Mo$: C, 50.97; H, 6.42. Found: C, 50.69; H, 6.52.

$(C_5Me_5)_2Gd(\mu\text{-}S)_2Mo(\mu\text{-}S)_2Gd(C_5Me_5)_2\cdot C_4H_8O$. This compound was prepared as described above for $(C_5Me_5)_2Y(\mu\text{-}S)_2Mo(\mu\text{-}S)_2Y(C_5Me_5)$ $(PPh_4)_2MoS_4$ (0.120 g, 0.133 mmol) and $(C_5Me_5)_2Gd(\mu\text{-}Ph)_2BPh_2$ (0.203 g, 0.272 mmol) were combined to yield dark purple solids of $(C_5Me_5)_2Gd(\mu\text{-}S)_2Mo(\mu\text{-}S)_2Gd(C_5Me_5)_2$ (0.120 g, 83%). Crystals suitable for single-crystal X-ray diffraction were grown from a concentrated toluene solution stored at −35 °C for 24 h. IR (cm^{-1}): 2901s, 2855s, 1591w, 1494m, 1433m, 1378m, 1189s, 1022w, 732m, 698m, 493s, 469m. Multiple elemental analyses are consistent with the inclusion of a THF molecule. Anal Calcd for $C_{40}H_{60}S_4Gd_2Mo\cdot C_4H_8O$: C, 45.89; H, 5.95. Found: C, 45.96; H, 5.96.

$(C_5Me_5)_2Tb(\mu\text{-}S)_2Mo(\mu\text{-}S)_2Tb(C_5Me_5)_2$. This compound was prepared as described above for $C_5Me_5)_2Y(\mu\text{-}S)_2Mo(\mu\text{-}S)_2Y(C_5Me_5)_2$: $(PPh_4)_2MoS_4$ (0.135 g, 0.150 mmol) and $(C_5Me_5)_2Tb(\mu\text{-}Ph)_2BPh_2$ (0.230 g, 0.307 mmol) were combined to yield the product as a purple powder (0.089 g, 55%). Crystals suitable for single-crystal X-ray diffraction were grown from a concentrated toluene solution stored at −35 °C for 24 h. IR (cm^{-1}): 2963s, 2900s, 2855s, 2725w, 2360m, 2341m, 2244m 2056w, 1435m, 1378m, 1022m, 732m, 489s, 478s, 434m. Anal Calcd for $C_{40}H_{60}S_4Tb_2Mo$: C, 44.36; H, 5.58. Found: C, 44.51; H, 5.58.

$(C_5Me_5)_2Dy(\mu\text{-}S)_2Mo(\mu\text{-}S)_2Dy(C_5Me_5)_2$. This compound was prepared as described above for $(C_5Me_5)_2Y(\mu\text{-}S)_2Mo(\mu\text{-}S)_2Y(C_5Me_5)_2$: $(PPh_4)_2MoS_4$ (0.142 g, 0.157 mmol) and $(C_5Me_5)_2Dy(\mu\text{-}Ph)_2BPh_2$ (0.243 g, 0.323 mmol) were combined to yield the product as a purple/brown powder (0.115 g, 67%). Crystals suitable for single-crystal X-ray diffraction were grown from a concentrated toluene solution stored at −35 °C for 24 h. IR (cm^{-1}): 2963s, 2901s, 2854s, 2724w, 1434m, 1431m, 1378m, 1022m, 733m. Anal Calcd for $C_{40}H_{60}S_4Dy_2Mo$: C, 44.07; H, 5.55. Found: C, 44.36; H, 5.41.

[Co(C5Me5)2][(C5Me5)2Y(μ-S)2Mo(μ-S)2Y(C5Me5)2], 1-Y. To a stirred solution of (C5Me5)2Y(μ-S)2Mo(μ-S)2Y(C5Me5)2 (0.082 g, 0.087 mmol) in 6 mL of THF was added Co(C5Me5)2 (0.027 g, 0.082 mmol) in 4 mL of THF. The solution changed from purple to red immediately. After 1 h, the solvent was removed under reduced pressure to produce a red solid. The solid was washed with toluene (3 × 2 mL) and dried under reduced pressure to yield the product as a red solid (0.077 g, 74%). Recrystallization of this solid from concentrated THF solutions at −35 °C for 24 h afforded red block-shaped crystals suitable for single-crystal X-ray diffraction. ^{1}H NMR (THF-d_8): δ 2.38 (s, br, 60H, C5*Me5*), 2.26 (s, br, 30H, Co(C5*Me5*)2). IR (cm^{-1}): 2957s, 2892s, 2851s, 2719w, 1475m, 1446m, 1427m, 1376m, 1259w, 1065m, 1022m. Anal Calcd for $C_{60}H_{90}S_4Y_2CoMo$: C, 56.64; H, 7.13. Found: C, 56.42; H, 7.19.

Scheme 1. Synthesis of (C5Me5)2Ln(μ-S)2Mo(μ-S)2Ln(C5Me5)2 and **1-Ln** (Ln = Y, Gd, Tb, Dy).

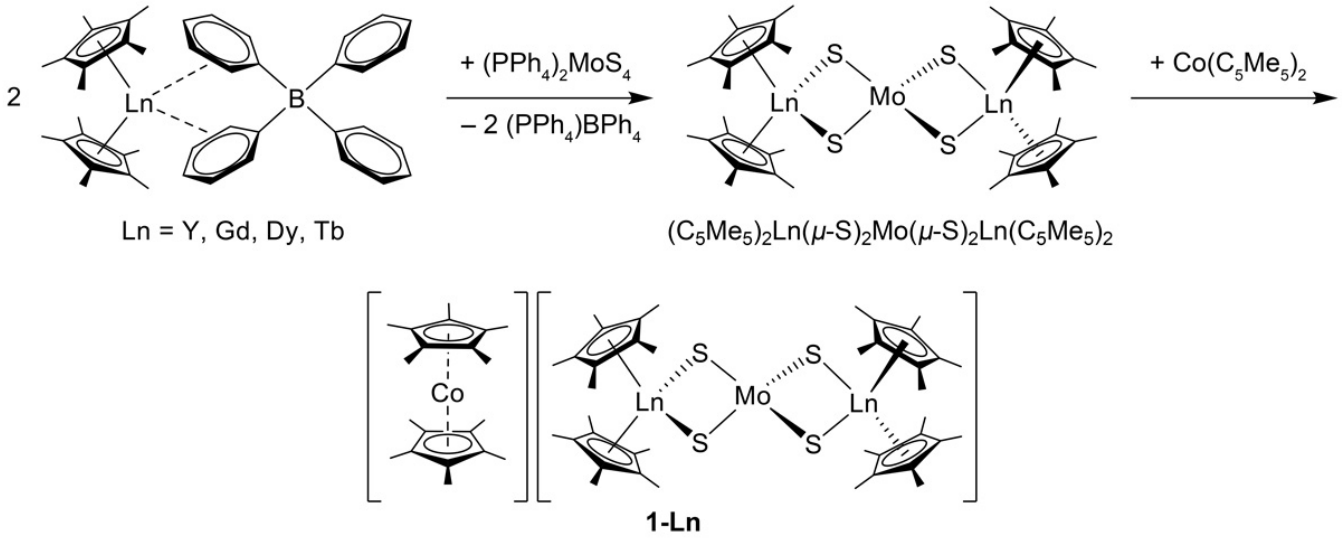

[Co(C5Me5)2][(C5Me5)2Gd(μ-S)2Mo(μ-S)2Gd(C5Me5)2], 1-Gd. This compound was prepared as described above for **1-Y**. (C5Me5)2Gd(μ-S)2Mo(μ-S)2Gd(C5Me5)2 (0.120 g, 0.111 mmol) and Co(C5Me5)2 (0.0350 g, 0.106 mmol) were combined in THF to yield a red solution. The THF was removed from this solution under reduced pressure to yield a red powder. Recrystallization from concentrated THF solutions at −35 °C for 24 h gave the product as red block-shaped crystals (0.087 g, 58%) suitable for single-crystal X-ray diffraction. IR (cm^{-1}): 2962m, 2888s, 2851s, 2721w, 1476m, 1450m, 1432m, 1388m, 1377m, 1066w, 1023m. Anal Calcd for $C_{60}H_{90}S_4Gd_2CoMo$: C, 51.15; H, 6.44. Found: C, 49.86; H, 6.32. Low carbon and hydrogen values were obtained even after multiple analysis attempts using different batches of samples. Found H/C ratios support an empirical formula having $C_{60}H_{90}$; this discrepancy may result from incomplete combustion of the material during the elemental analysis experiment determination.

[Co(C5Me5)2][(C5Me5)2Tb(μ-S)2Mo(μ-S)2Tb(C5Me5)2], 1-Tb. This compound was prepared as described above for **1-Y**. (C5Me5)2Tb(μ-S)2Mo(μ-S)2Tb(C5Me5)2 (0.089 g, 0.084 mmol) and Co(C5Me5)2 (0.026 g, 0.079 mmol) were combined in THF to yield a red solution. The THF was removed from this solution under reduced pressure to yield a red powder. Recrystallization from concentrated THF solutions at −35 °C for 24 h afforded the product as red block-shaped crystals (0.041 g, 37%) suitable for single-crystal X-ray diffraction. IR (cm^{-1}): 2961m, 2889s, 2851s, 2718w, 1476m, 1449m, 1428m, 1385s, 1377s, 1066m, 1024m. Anal Calcd for $C_{64}H_{98}S_4OTb_2CoMo$: C, 51.78; H, 6.65. Found: C, 52.05; H, 6.42.

[Co(C5Me5)2][(C5Me5)2Dy(μ-S)2Mo(μ-S)2Dy(C5Me5)2], 1-Dy. This compound was prepared as described above for **1-Y**. (C5Me5)2Dy(μ-S)2Mo(μ-S)2Dy(C5Me5)2 (0.119 g, 0.109 mmol) and Co(C5Me5)2 (0.037 g, 0.112 mmol) were combined in THF to yield a red solution. The THF was removed from this solution under reduced pressure to yield a red powder. Recrystallization from concentrated THF solutions at −35 °C for 24 h afforded the product as red block-shaped crystals (0.055 g, 35%) suitable for single-crystal X-ray diffraction. IR (cm^{-1}): 3372w, 2960s, 2889s, 2852s, 2722m, 2361m, 2344m, 1475m, 1447m, 1428m, 1377m, 1024m, 732m, 434s. Anal Calcd for $C_{64}H_{98}S_4ODy_2CoMo$: C, 51.53; H, 6.62. Found: C, 51.49; H, 6.79.

RESULTS AND DISCUSSION

Synthesis and Structural Characterization. The tetrathiomolybdate unit, MoS_4^{y-}, has previously been shown to bridge multiple metal centers in transition metal complexes containing Cu,[15] Fe,[16] and Nb,[17] which have primarily found interest in nonlinear optics and as models for the Fe-Mo cofactor in the enzyme nitrogenase. The compound (PPh4)[(C5Me5)2Sm(μ-S)2Mo(μ-S)2Sm(C5Me5)2], which contains an S = ½ MoS_4^{3-} unit bridging two Sm^{III} centers, has also been previously synthesized, demonstrating the ability of a MoS_4^{y-} unit to bridge two lanthanide(III) centers.[18] Since the later lanthanides are known to facilitate magnetic exchange and slow magnetic relaxation via their large magnetic moments and magnetic anisotropies, we chose to pursue analogous complexes with Gd, Tb, and Dy.

Toward this goal, the purple trimetallic MoS_4^{2-} bridged complexes (C5Me5)2Ln(μ-S)2Mo(μ-S)2Ln(C5Me5)2 (Ln = Y, Gd, Tb, Dy) were synthesized according to the first step of Scheme 1. Single-crystal X-ray diffraction of these compounds revealed two Ln^{III} centers, each capped by two pentamethylcyclopentadienyl ligands, bridged by a MoS_4^{2-} ion with a pseudo-tetrahedral, diamagnetic Mo^{VI} center (Table S1). One-electron reduction of these compounds using decamethylcobaltocene, Co(C5Me5)2, −1.94 V vs.

$[Cp_2Fe]^{0/1+}$),[19] resulted in a red powder that could be isolated directly from the THF reaction mixture after removing the solvent under reduced pressure. Cooling a concentrated THF solution of this solid to −35 °C overnight afforded X-ray diffraction-quality crystals and enabled structural characterization of $[Co(C_5Me_5)_2][(C_5Me_5)_2Ln(\mu$-

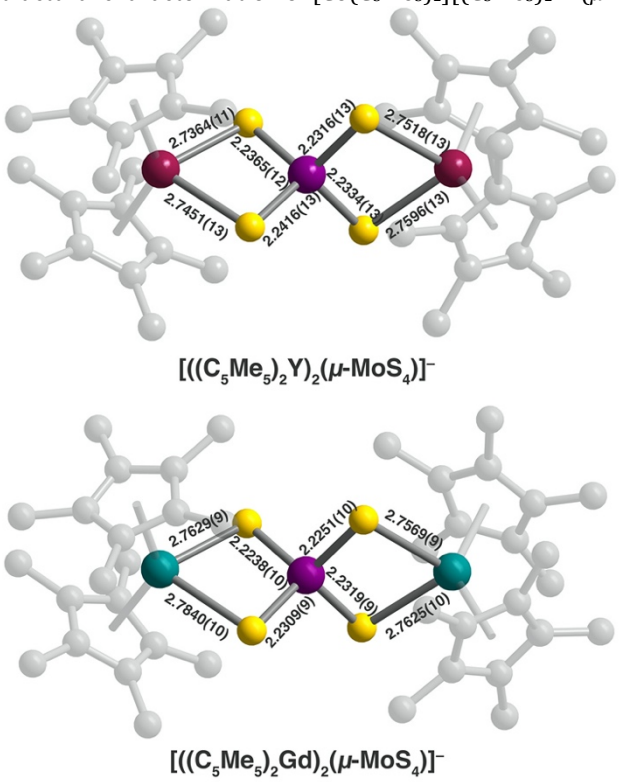

Figure 1. Top: Structure of the MoS_4^{3-}-bridged diyttrium complex anion in **1-Y**. Compounds **1-Tb** and **1-Dy** are isostructural with **1-Y**. Bottom: Structure of the MoS_4^{3-}-bridged digadolinium complex anion in **1-Gd**. Relevant bond lengths in units of Å are overlaid. Maroon, cyan, purple, yellow, and grey spheres represent Y, Gd, Mo, S, and C atoms, respectively; H atoms and a $[Co(C_5Me_5)_2]^+$ countercation, and cocrystallized solvent molecules are omitted for clarity. C_5Me_5 substituents are faded to aid visualization of the $MoLn_2$ core.

$S)_2Mo(\mu$-$S)_2Ln(C_5Me_5)_2]$ (Ln = Y, Gd, Tb, Dy), **1-Ln** (Figure S1 and Table S2).

In the structure of **1-Gd** (Figure 1), the two Gd^{III} centers are inequivalent by symmetry, with two unique Gd···Mo distances of 3.4378(3) and 3.4419(3) Å. The Mo–S bond lengths support the occurrence of a Mo-centered reduction, with the average Gd–S bond lengthening from 2.1906(12) Å in $(C_5Me_5)_2Gd(\mu$-$S)_2Mo(\mu$-$S)_2Gd(C_5Me_5)_2$ to 2.2278(10) Å upon reduction to **1-Gd**. The tetrahedral MoS_4 unit is compressed along the Gd···Gd axis, resulting in S–Mo–S angles of 110.96(4)°, 110.72(4)°, 106.49(4)°, and 106.65(4)°. The axis and degree of distortion of the MoS_4 tetrahedron is consistent across the **1-Ln** series. Comparing the structure of **1-Gd** with that of **1-Y** reveals several differences (Figure 1). While the Mo–S bond lengths in **1-Gd** are all relatively similar, those of **1-Y** exhibit distinct asymmetry. On one side of the molecule, long Mo–S bonds are observed, with an average bond length of 2.2391(13) Å, in addition to short Ln–S bond lengths, averaged to 2.7408(12) Å. On the opposite side, short Mo–S bonds, averaging to 2.2325(13) Å, and long Ln–S bonds, averaging to 2.7557(13) Å, are observed. This asymmetry may suggest some localization of the unpaired Mo^V electron on one side of the molecule. Since the Mo^V-centered unpaired electron populates a Mo–S antibonding orbital, Mo–S bond lengths should increase on the side of the charge localization, while Ln–S bonds on the same side may be expected to decrease due to an Ln–MoS_4 bonding-type interaction. The structures of **1-Tb** and **1-Dy** are isostructural with that of **1-Y** and show a similar asymmetry of the Mo–S and Ln–S bond lengths.

EPR Spectroscopy. The EPR spectrum for **1-Y** collected at 77 K in frozen THF (Figure 2) shows a primary signal consistent with an $S = {}^1/_2$ Mo^V center (^{95}Mo, $I = 0$, 75% abundance; ^{97}Mo, $I = {}^5/_2$, 25% abundance). The spectrum can only be reasonably fit[20] when including hyperfine coupling to a single ^{89}Y center ($I = {}^1/_2$, 100% abundance), rather than coupling to both ^{89}Y centers. Three g values of $g_x = 1.972$, $g_y = 1.980$, and $g_z = 1.988$ were included in the fit, along with three ^{95}Mo coupling constants, both sets of which are consistent with reported Mo^V EPR spectra (Tables S3 and S4).[16,17] In contrast, the ^{89}Y hyperfine coupling constants of $A_\perp = 23$ MHz, and $A_{||} = 26$ MHz are substantially larger than previously observed yttrium-transition metal hyperfine couplings,[21] suggesting a non-negligible electron delocalization from the MoS_4^{3-} unit onto one of the Y centers. Indeed, the divalent yttrium compound $[K(2.2.2\text{-cryptand})][(C_5H_4SiMe_3)_3Y]$, with a single electron localized in a $5d_{z^2}$ orbital, exhibits an only four-fold higher hyperfine coupling of $A_{iso} = 102.6$ MHz.[23]

The observed charge transfer involving only a single yttrium center has at least two potential explanations. First is the disproportionation of **1-Y** in THF solution to form a complex in which only a single $[(C_5Me_5)_2Y]^+$ cation is bound to the $(MoS_4)^{3-}$ ligand, resulting in an EPR spectrum reflective of only one Mo^V-Y^{III} interaction. Second is a charge localization on one half of the $(MoS_4)^{3-}$ ligand, potentially supported by the observed asymmetry of Mo–S and Y–S bond distances described above, leading to two distinct Mo···Y separations of 3.4320(5) Å and 3.4263(6) Å. The

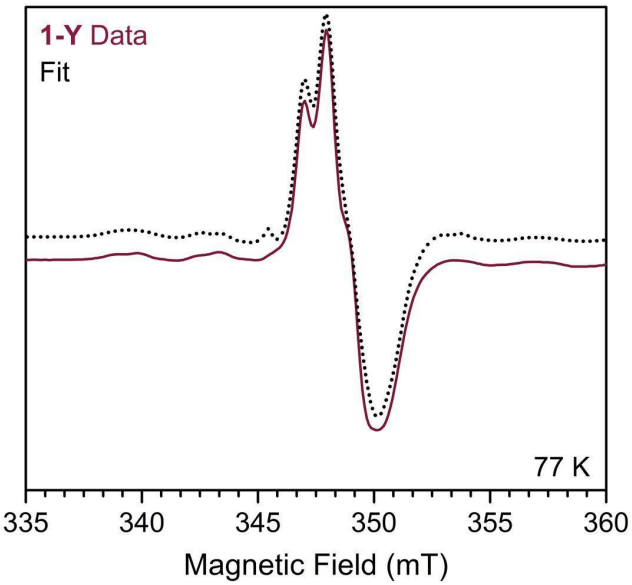

Figure 2. X-band EPR spectrum of **1-Y** in frozen THF solution, collected at 77 K. The dotted black line represents a fit to the data, shown as a maroon line, as described in the text and Supporting Information. Fitting parameters are shown in Table S3.

shorter Mo···Y distance corresponds to longer Mo–S and shorter Y–S average distances, potentially demarcating this side of the molecule as the charge transfer pathway (Figure 1).

Considering the character of the filled Mo^{V} orbital, and thus the mechanism of Mo–Ln charge transfer, the observation from the EPR spectrum that $g_z > g_x, g_y$ suggests that the d_{z^2} orbital is populated.[24] In principle, the crystallographic parameters for the MoS_4^{3-} unit can be assessed to determine the nature and orientation of the d orbital. Here, if the d_{z^2} orbital is populated, the MoS_4^{3-} unit should be elongated along the z axis due to a Jahn-Teller distortion away from T_d symmetry.[25] Across the series **1-Ln**, the MoS_4^{3-} tetrahedron is elongated perpendicular to the Ln···Ln axis. However, the MoS_4^{2-} tetrahedra in $(C_5Me_5)_2Ln(\mu\text{-}S)_2Mo(\mu\text{-}S)_2Ln(C_5Me_5)_2$ are distorted to a similar degree along the same axis, suggesting that any MoS_4^{3-} distortion away from tetrahedral symmetry is a consequence of the coordination of two $[(C_5Me_5)_2Ln]^{1+}$ units, rather than a Jahn-Teller perturbation. The Mo^{V}-based unpaired electron can therefore be attributed to a d_{z^2} orbital with the z axis lying parallel to the Ln···Mo···Ln axis, in agreement with molecular orbital analysis of a known trinuclear MoS_4^{n-}-bridged complex.[16b]

Electronic Structure Calculations. To corroborate this assessment, all electronic structure calculations for the **1-Ln** series were performed on Turbomole program suite version V7.4 using scalar-relativistic small-core effective core potentials for the lanthanide atoms and the TPSSh hybrid meta-GGA functional (see Supporting Information for details). [26] Calculations were performed on compound **1-Ln** as well as two simplified model complexes; here **[1-Ln]**$^-$ refers to the anionic model complex $[C_5Me_5)_2Ln(\mu\text{-}S)_2Mo(\mu\text{-}S)_2Ln(C_5Me_5)_2]^-$ and **[1'-Ln]**$^-$ refers to the further simplified anionic model complex $[C_5H_5)_2Ln(\mu\text{-}S)_2Mo(\mu\text{-}S)_2Ln(C_5H_5)_2]^-$. Compounds **[1-Ln]**$^-$ were all found to exhibit ground state equilibrium structures with C_2 point group symmetry (Tables S16 and S17). The singly occupied A-symmetric HOMO of **[1-Y]**$^-$**,** Figure 3, corresponds to an Mo^{V} $4d_{z^2}$ orbital parallel to the Y···Mo···Y axis, and coupled with $4d_{z^2}$

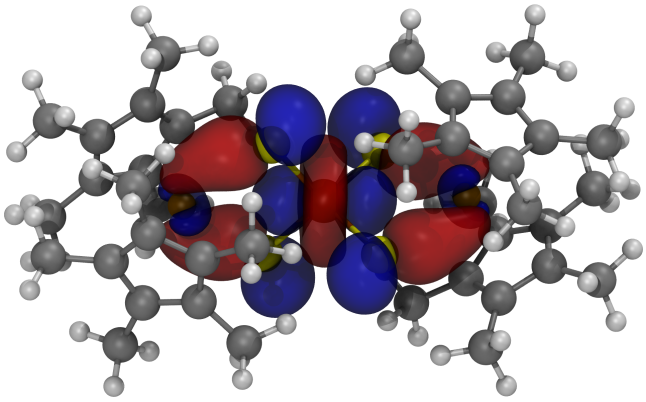

Figure 3. HOMO of the C_2 symmetry-optimized anionic **[1-Y]**$^-$ model complex (TPSSh-D3, def2-TZVP (Mo, Y, S), def2-SVP (C, H)) (see Supporting Information for further computational details). The calculated HOMO picture confirms the proposed primary magnetic coupling pathway in **1-Ln** of Mo-$4d_{z^2}$ to Ln-$5d_{z^2}$. Color scheme: H=white, C=gray, S=yellow, Mo=light brown, Y=dark brown, isovalue=±0.025.

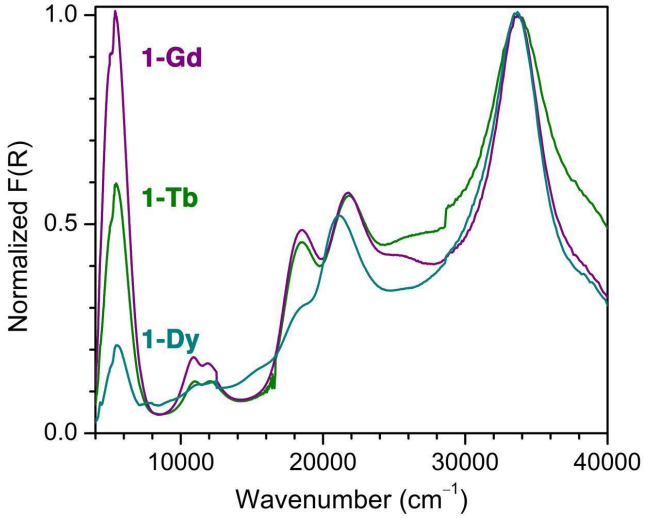

Figure 4. Normalized diffuse reflectance UV-Vis-NIR spectra for **1-Gd**, **1-Tb**, and **1-Dy**, shown in purple, green, and blue, respectively. F(R) is a Kubelka-Munk conversion of the raw diffuse reflectance spectrum. Spectra are normalized with the strongest absorbance set to F(R) = 1.

orbitals of the Y atoms through bridging sulfur d orbitals (Tables S10 and S11). The totally symmetric HOMOs of [**1-Gd**]$^-$, [**1-Tb**]$^-$, and [**1-Dy**]$^-$ involve Ln $5d_{z^2}$ orbitals, but are otherwise similar to **[1-Y]**$^-$ (Figures S4-S10).

To explore the origin of the slight asymmetry observed in the experimental X-ray structures, the possibility of symmetry-breaking distortions was investigated computationally. All ground-states are non-degenerate, excluding the possibility of first-order Jahn-Teller distortion, whereas second-order (pseudo) Jahn-Teller distortion was ruled out by vibrational analysis (Table S9). Comparison to the simplified model system **[1'-**

Y]$^-$, which has comparatively high D_{2d} symmetry, shows that the lowering of the symmetry is due to steric effects of the ligands rather than electronic effects (Figure S2, Tables S5-S11). Geometry optimization of **1-Y**, which includes the decamethylcobaltocenium counterion, yielded structural distortions similar to those observed in the experimental **1-Y** crystal structure (Table S12), although the electronic structure showed insignificant changes (Figure S3, Tables S10-S11 vs. S13-S14), suggesting electrostatic polarization as the main cause of the distortion. Nevertheless, the computed spin densities at the position of the two inequivalent Y atoms do differ slightly in **1-Y** calculations (Table S15), consistent with the hypothesis of some charge localization on one side of the molecule.

UV-Vis-NIR Spectroscopy. UV-Vis-NIR diffuse reflectance measurements of **1-Ln** (Figure 4) exhibit a number of features consistent with a $(MoS_4)^{3-}$ unit.[21c] For example, **1-Gd** exhibits transitions at 33675 cm^{-1} and 21789 cm^{-1}, assigned to LMCT (S→Mo) t_2→e and t_1→e transitions, respectively, 18486 cm^{-1}, tentatively assigned to a triplet charge transfer transition,[27] and 11977 cm^{-1} and 10895 cm^{-1}, assigned to Mo^V ligand field e→t_2 transitions, approximating the symmetry of the MoS_4^{3-} tetrahedron as T_d. In addition, an intense near-IR feature is observed at 5397 cm^{-1}, which is assigned to a metal-to-metal charge transfer transition (MMCT; Mo→Ln). The MMCT transition increases slightly in energy to 5444 cm^{-1} and 5559 cm^{-1} for **1-Tb** and **1-Dy**, respectively, and diminishes substantially in intensity from **1-Gd** to **1-Tb** to **1-Dy**, trending with the decreasing size of the lanthanide ionic radii.

Time-dependent density functional calculations support this assignment. Simulated absorption spectra for **[1-Ln]**$^-$ show all experimentally observed features, although the relative intensity of the MMCT band is underestimated, and the position is shifted to higher wavenumbers (Figures S11-S14 and Tables S18-21).

Metal-to-metal charge transfer involving a lanthanide ion is exceedingly rare, with other reported examples occurring at much higher energies with much lower intensity.[28] The low energy of the MMCT transition can be ascribed to the highly reducing nature of the Mo^V ion, which should have a decent energy match with the Ln^{III}/Ln^{II} reduction potential. Further, strong-field cyclopentadienyl ligands have been shown to preferentially stabilize the lanthanide $5d_{z^2}$ orbital,[23] and as such the $5d_{z^2}$ orbital in these organometallic complexes should be more accessible compared to complexes with Ln^{III} ions in weaker ligand fields. The low-energy MMCT indicates that **1-Ln** may have accessible Ln^{III}/Ln^{II} reduction potentials that permit isolation of derivatives with Ln^{II} centers; this avenue will be explored in future work.

Magnetic Measurements. Variable-temperature dc magnetic susceptibility measurements were performed from 2–300 K to investigate the presence and nature of magnetic communication between the lanthanide centers and Mo^V in **1-Gd**, **1-Tb**, and **1-Dy**. For **1-Gd**, the product of magnetic susceptibility times temperature, $\chi_M T$, at 300 K was found to be 19.1 emu K/mol under an applied field of 0.1 T (Figure 5). This value is higher than the expected 16.135 emu K/mol for two magnetically isolated $S = {}^7/_2$ Gd^{III} centers and an $S = {}^1/_2$ Mo^V center, suggesting the presence of significant ferromagnetic Gd–Mo exchange. Indeed, $\chi_M T$ for **1-Gd** rises steadily with decreasing temperature until reaching a maximum value of 31.6 emu K/mol at 6 K, in good agreement with the expected value of 31.875 emu K/mol for an $S = {}^{15}/_2$ ground state. The small downturn in the $\chi_M T$ product below 6 K can be ascribed to Zeeman splitting of this high-spin ground state.

The nature and strength of the Gd–Mo magnetic coupling were evaluated by fitting the $\chi_M T$ data[29] using the following Hamiltonian:

$$\hat{H} = -2(J_{Gd-Mo})(\hat{S}_{Mo} \cdot (\hat{S}_{Gd(1)} + \hat{S}_{Gd(2)})) + \sum_{i=Gd,Mo} \mu_B \hat{S}_i g_i H \qquad (1)$$

where J_{Gd-Mo} is the Gd–Mo magnetic coupling constant. Good agreement between data and fit was obtained using a J_{Gd-Mo} value of +16.1(2) cm^{-1}, along with a χ_{TIP} contribution of 0.0053(2) emu/mol. Remarkably, the J_{Gd-Mo} value represents one of the largest exchange constants observed to date between Gd^{III} and another spin center. The record value of J_{Gd-e^-} = +175(10) cm^{-1} was recently determined for coupling between Gd^{III} and a radical "trapped" in a metal-

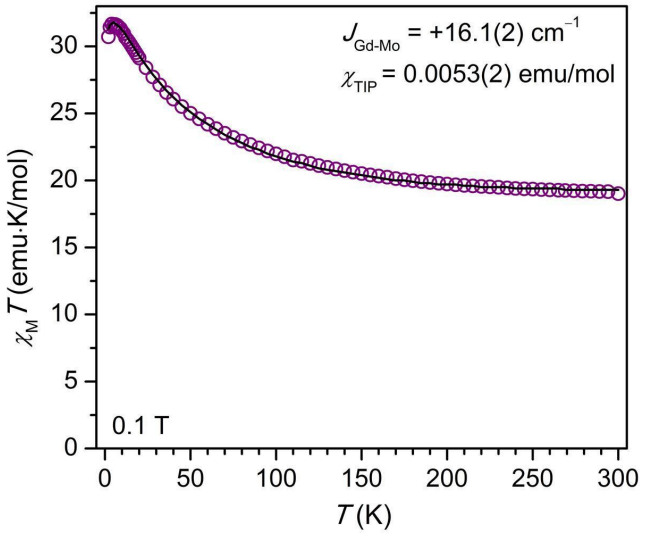

Figure 5. Plot of the magnetic susceptibility times temperature product ($\chi_M T$) versus temperature for **1-Gd**. Purple circles represent data collected under an applied magnetic field of 0.1 T, and the black line represents a fit to the data using the Hamiltonian in Equation 1.

metal bonding-type orbital in $Gd_2@C_{79}N$,[30] and is followed in magnitude by coupling constants of $J = -27$ cm^{-1} [2a,31] and -20 cm^{-1} [3] determined for the interaction between Gd^{III} and an N_2^{3-} radical bridge. Notably, the extracted Gd–Mo coupling is the strongest yet observed between gadolinium and a transition metal center, superseding the previous record of +10.1 cm^{-1} for a Gd–Cu complex.[32] As expected for a strongly exchange-coupled complex, low-temperature magnetization versus applied magnetic field curves collected from 2–10 K agree well with simulated Brillouin

curves for a $S = {}^{15}/_{2}$ ground state with $g = 2.05$ (Figure S15).

The strong Gd–Mo charge-transfer exchange interaction can be attributed to a number of factors. First and most simply, the more diffuse character of the 4d orbitals relative to those of the 3d transition metal series should promote enhanced orbital interactions with the empty 5d orbitals of the lanthanides, while the higher energy of the 4d orbitals should enable better energy matching with the lanthanide 4f orbitals. However, given the small Ln–Mo couplings observed for cyano-bridged complexes, the nature of the bridging thiometallate in **1-Gd** must also be considered essential to achieving strong coupling. The close Gd•••Mo distance of ~3.43 Å facilitated by the single-atom sulfide bridges is likely the primary aid in enhancing magnetic interactions. Indeed, Gd^{III}–Mo^{V} interactions across larger distances have been shown to be quite weak, as exemplified by a value of $J_{Gd-Mo} = -0.68$ cm^{-1} for an $[Gd^{III}Mo^{V}(CN)_8]$ chain compound with a Gd•••Mo separation of 5.7 Å.[8d] The diffuse and polarizable nature of the S^{2-} bridges should additionally enable enhanced spin polarization compared to cyanide ligands; the sulfide ligands of thiometallate units have been previously shown to support substantial charge and spin delocalization.[33] Finally, despite the relatively short Gd•••Mo distance in **1-Gd**, the overlap integral between the Mo^{V} 4d and Ln^{III} 5d orbitals is still likely to be quite small, leading to an ideal

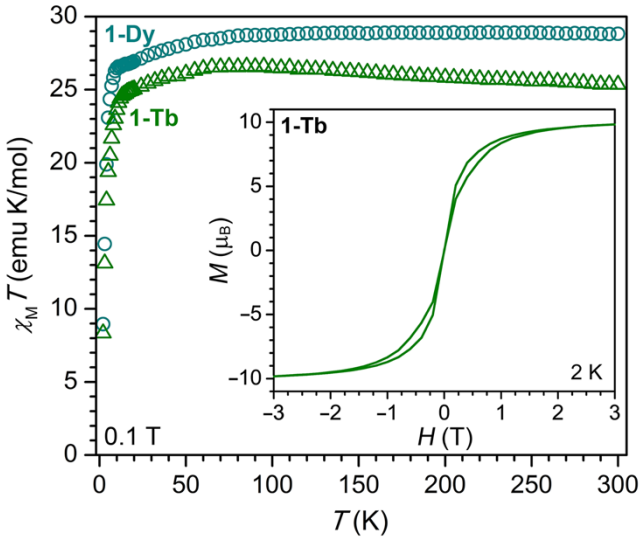

Figure 6. Magnetic susceptibility times temperature products ($\chi_M T$) versus temperature of **1-Tb** and **1-Dy**, represented by green triangles and cyan circles, respectively, collected under an applied magnetic field of 0.1 T. Inset: Magnetization versus applied magnetic field curve for **2-Tb** collected at 2 K with a field sweep rate of 0.4 mT s^{-1}.

scenario for charge transfer-driven ferromagnetic coupling—i.e., charge transfer from a SOMO of MoS_4^{3-} to an empty Gd^{III} 5d orbital, with minimal to no SOMO/SOMO overlap.[34]

At 300 K and under an applied field of 0.1 T, the $\chi_M T$ product for **1-Tb** is 25.35 emu K/mol, slightly higher than the expected value of 24.015 emu K/mol for two magnetically isolated Tb^{III} centers and an $S = {}^{1}/_{2}$ Mo^{V} center (Figure 6). This $\chi_M T$ value, in conjunction with the steady rise in $\chi_M T$ with decreasing temperature and corresponding absence of a local minimum, supports the presence of ferromagnetic interactions between spins, analogous to **1-Gd**. However, $\chi_M T$ increases only slightly to a maximum of 26.59 emu K/mol at 85 K, potentially indicating that Ln–Mo coupling is weak relative to that present in **1-Gd**. Thermal depopulation of Tb^{III} m_J levels is also expected to drive decreasing $\chi_M T$ with decreasing temperature for **1-Tb**, which may convolute any impacts of magnetic exchange on $\chi_M T$. Similarly, $\chi_M T$ at 300 K under an applied field of 0.1 T for **1-Dy** is 28.82 emu K/mol, also close to the expected value of 28.615 emu K/mol for two magnetically isolated Dy^{III} centers and an $S = {}^{1}/_{2}$ Mo^{V} center. The slightly higher than expected $\chi_M T$ value again supports the presence of ferromagnetic interactions. Negligible increase in the $\chi_M T$ product of **1-Dy** with decreasing temperature indicates even further reduced strength of magnetic exchange relative to **1-Gd** and **1-Tb**. The inferred trend in magnetic exchange strength, $J_{Gd\text{-}Mo} > J_{Tb\text{-}Mo} > J_{Dy\text{-}Mo}$, can be explained by the decrease in size of the lanthanide ionic radii and thereby diminished strength of metal-ligand and metal-metal interactions, in agreement with the decrease in MMCT transition intensity observed from **1-Gd** to **1-Dy** in UV-Vis-NIR spectra. The decrease in $\chi_M T$ observed for both **1-Tb** and **1-Dy** at low temperatures is attributed to thermal depopulation of exchange-coupled and crystal-field-split states.

Finally, **1-Tb** and **1-Dy** were investigated using ac magnetic susceptibility measurements to probe the possible presence of slow magnetic relaxation. We note that while magnetic coupling of metal centers can in principle generate a well-isolated, large-spin ground state conducive to slow magnetic relaxation under zero applied magnetic field, only a few 4f-*n*d (n = 4, 5) molecular complexes have actually been found to exhibit slow magnetic relaxation.[9] Variable-temperature ac magnetic susceptibility data were collected for **1-Tb** and **1-Dy** under zero dc field using a 4-Oe field oscillating at frequencies ranging from 1 to 1500 Hz. Between 2 and 13 K, both **1-Tb** (Figure S16) and **1-Dy** (Figure 7, top) exhibit asymmetric peaks in the out-of-phase susceptibility, χ'', indicative of slow magnetic relaxation. Cole-Cole plots of the in-phase susceptibility, χ', versus the out-of-phase susceptibility, χ'', appear as broad and asymmetric semicircles, suggesting the overlap of more than one time regime for the magnetization relaxation and hence more than one relaxation process. The severity of this overlap precluded extraction of precise relaxation time data for distinct processes (Figure S17), and instead the Cole-Cole plot data for both compounds were approximately fit using a single modified Debye model,[1a] yielding values for the relaxation time, τ, at each temperature. Among the resulting fitted parameters is the α value, which provides a measure of the uniformity of relaxation and ranges from 0 to 1, with smaller values corresponding to relaxation dominated by a single process. Values of α as high as 0.4-0.5 at the lowest temperatures for both **1-Tb** and **1-Dy** confirm the presence of multiple relaxation processes.

To gain insight into the nature of the slow magnetic

relaxation exhibited by **1-Tb**, we examined the temperature dependence of the natural log of the relaxation times (Figure S18) and found pronounced curvature instead of the Arrhenius behavior of a thermally-activated over-barrier relaxation process. The temperature dependence of τ was best fit using the expression $\tau^{-1} = CT^n$, with C = 12.3 s^{-1} K^{-n} and n = 2.5 (Figure S18), indicating that at least one Raman relaxation mechanism, a spin–lattice relaxation process that occurs through virtual magnetic excited states, likely dominates in the examined temperature and frequency range. Under an applied field between 2 and 5 K, the relaxation time of **1-Tb** is also sufficiently long to observe waist-restricted magnetic hysteresis (Figure 6, inset, and Figure S19).

In contrast, no magnetic hysteresis was observed for **1-Dy** using the same field sweep rate and for temperatures as low as 2 K (Figure S22), although this compound exhibits ac peaks over a similar temperature and frequency range as **1-Tb** (Figures 7, S20, and S21). Relaxation times extracted from ac magnetic susceptibility data suggest that slow magnetic relaxation for **1-Dy** arises due to both Raman relaxation and thermally-activated Orbach relaxation. Accordingly, an Arrhenius plot of the relaxation times could be fit to the equation:

$$\tau^{-1} = CT^n + \tau_0^{-1} \, exp \, exp \left(-\frac{U_{eff}}{k_B T}\right) \qquad (2)$$

with C = 10.2 s^{-1} K^{-n}, n = 2.2, τ_0 = 5.7 x 10^{-9} s, and U_{eff} = 68 cm^{-1} (Figure 7, bottom). It is possible that the barrier to magnetization reversal exhibited by **1-Dy** derives from Dy^{III} single-ion anisotropy, as opposed to the energy landscape of the total coupled system, although the present data do not allow for a definitive determination. Nevertheless, the barrier of U_{eff} = 68 cm^{-1} is the highest yet observed for any complex containing a lanthanide ion and paramagnetic 4d metal center.[9] Moreover, the barrier for **1-Dy** is the highest for any complex simply containing a paramagnetic 4d metal center.[7] We also note that a temperature-independent regime is not observed in the Arrhenius plot for either **1-Tb** or **1-Dy**, indicating the

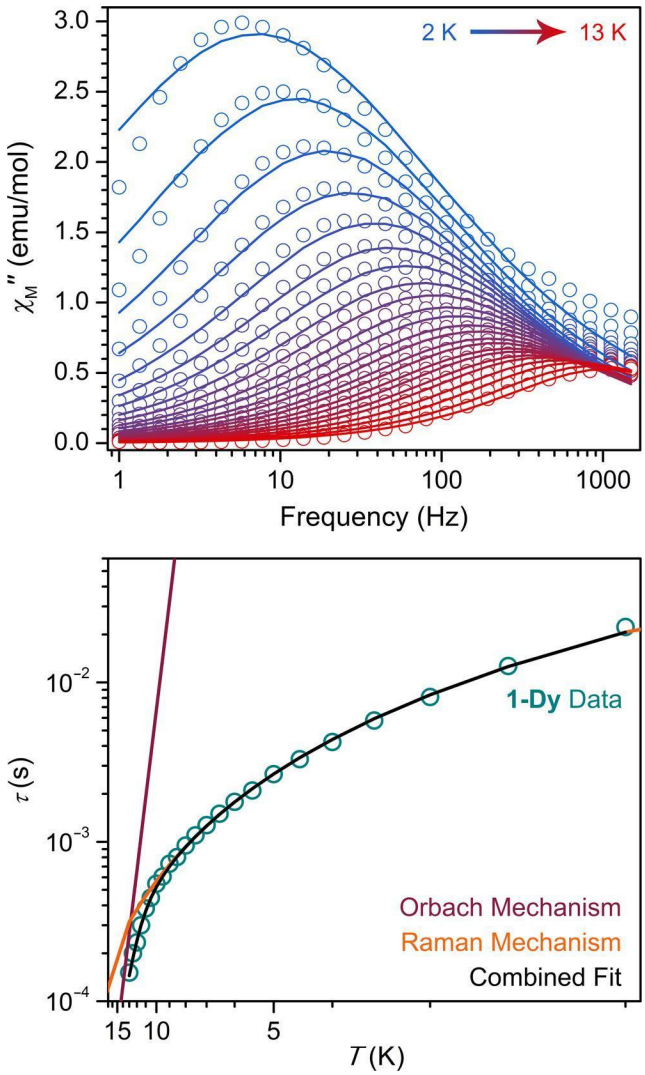

Figure 7. Top: Variable-temperature out-of-phase magnetic susceptibility versus frequency data for **1-Dy**, collected at temperatures ranging from 2 to 13 K under zero applied magnetic field. Colored symbols represent data points and lines represent fits of the data to a generalized Debye model. Bottom: Arrhenius plot of magnetic relaxation times, τ (log scale) versus temperature (inverse scale) for **1-Dy**. Data are represented by cyan circles. Orange and maroon lines represent the Raman and Orbach components, respectively, of the fit to the data, while the black line represents the total fit to Equation 3, as described in the text, giving values of C = 10.2 s^{-1} K^{-n}, n = 2.2, τ_0 = 5.7 x 10^{-9} s, and U_{eff} = 68 cm^{-1}.

absence of any detrimental zero-field tunneling behavior, possibly inhibited by Ln^{III}–Mo^{V} exchange.[4a,35]

The absence of large barriers to magnetic relaxation in both **1-Tb** and **1-Dy** likely arises due to the misalignment of magnetic anisotropy axes. Since the strongly donating $(C_5Me_5)^{1-}$ ligands should define the magnetic axis of each lanthanide (assuming an oblate electronic state)[36,37] and the $(C_5Me_5)^{1-}$ ligands on each lanthanide in **1-Tb** and **1-Dy** are in planes roughly perpendicular to one another, the anisotropy axes of the lanthanide centers are likely close to perpendicular. Systems containing magnetic ions with non-collinear magnetic axes typically exhibit mixed-axiality ground states, which enable quantum tunneling of magnetization as well as low-lying excited states.[38] Improved single-molecule magnet behavior could be achieved via rational synthesis of a molecule with collinear lanthanide anisotropy axes, in which both lanthanides can strongly engage in 4f/5d-*n*d interactions. With this in mind, we are now pursuing dilanthanide molecules incorporating octahedral or square planar 4d or 5d complexes with single-atom bridging ligands that should enable strong magnetic exchange.

CONCLUSIONS AND OUTLOOK

Mechanisms of *n*d-4f magnetic exchange have long captivated the molecular magnetism community.[39] The foregoing results demonstrate for the first time that 4d, and likely 5d, metal centers can achieve strong magnetic interactions with lanthanide ions in molecular complexes. Polarizable bridging ligands that facilitate charge and spin transfer and sufficiently short lanthanide-transition metal distances play crucial roles in the strength of magnetic exchange. Strong ferromagnetic coupling is observed for **1-Gd**, giving rise to the largest molecular lanthanide-transition metal exchange coupling constant observed to date, J = +16.1(2) cm^{-1}. Compounds **1-Tb** and **1-Dy** also exhibit slow magnetic relaxation, with the latter compound displaying a relaxation barrier of U_{eff} = 68 cm^{-1}, the largest such value yet observed for both a 4f-4d complex and any 4d-metal-containing complex. Together, these results highlight new strategies with which to achieve strong magnetic exchange with the lanthanide ions, and suggest the possibility to access higher-barrier *n*d-4f single-molecule magnets via enhanced *n*d-4f magnetic exchange.

SUPPORTING INFORMATION

The Supporting Information is available free of charge on the ACS Publications website.
Additional experimental procedures, X-ray crystallographic information, additional spectroscopic and magnetic data, computational information. (PDF)

AUTHOR INFORMATION

Corresponding Authors

William J. Evans – *Department of Chemistry, University of California, Irvine, California 94697, United States*; orcid.org/ 0000-0002-0651-418X
Email: wevans@uci.edu

Jeffrey R. Long – *Department of Chemistry, University of California, Berkeley, California 94720, United States;* orcid.org/0000-0002-5324-1321
Email: jrlong@berkeley.edu,

Authors

Lucy E. Darago – *Department of Chemistry, University of California, Berkeley, California 94720, United States;* orcid.org/0000-0001-7515-5558

Monica D. Boshart – *Department of Chemistry, University of California, Irvine, California 94697, United States;* orcid.org/0000-0002-5377-1322

Brian D. Nguyen – *Department of Chemistry, University of California, Irvine, California 94697, United States*; orcid.org/0000-0001-7713-1912

Eva Perlt - *Department of Chemistry, University of California, Irvine, California 94697, United States*; orcid.org/ 0000-0002-4670-0542

Joseph W. Ziller – *Department of Chemistry, University of California, Irvine, California 94697, United States*; orcid.org/0000-0001-7404-950X

Wayne Lukens – *Chemical Sciences Division, Lawrence Berkeley National Laboratory, Berkeley, California 94720, United States;* orcid.org/0000-0002-0796-7631

Filipp Furche – *Department of Chemistry, University of California, Irvine, California 94697, United States*; orcid.org/0000-0001-8520-3971

Author Contributions

‡These authors contributed equally.

Notes

The authors declare no competing financial interest.

ACKNOWLEDGMENTS

We thank the U. S. National Science Foundation for support of this research through grants CHE-1855328 (W.J.E) and CHE-1800252 (J.R.L.). E.P. gratefully acknowledges funding by the German Research Foundation (DFG) through Project No. 391320977. This material is based upon work supported by the U.S. Department of Energy, Office of Basic Energy Sciences, under Award Number DE-SC0018352. Computations were supported by the Research Cyberinfrastructure Center at the University of California, Irvine, under Grant No. CNS-1828779. Analysis of the EPR spectrum (W.W.L.) was supported by the U.S. Department of Energy, Office of Science, Basic Energy Sciences, Chemical Sciences, Biosciences, and Geosciences Division, Heavy Element Chemistry Program and was performed at Lawrence Berkeley National Laboratory under contract No. DE-AC02-05CH11231. Single-crystal X-ray diffraction data for **1-Gd** were collected on Beamline 12.2.1 at the Advanced Light Source, which is supported by the Director, Office of Science, Office of Basic Energy Sciences, of the U.S. Department of Energy under Contract no. DE-AC-02-05CH11231. We thank the NSF Graduate Research Fellowship Program for support of L.E.D. We also thank Dr. Jason R. Jones, Michael K. Wojnar, and Ari Turkiewicz for assistance with X-ray crystallography, Professor Alan F. Heyduk and Alexandre Vincent for helpful discussions, and Dr. Katie Meihaus for editorial assistance.

REFERENCES

(1) (a) Gatteschi, D., Sessoli, R., Villain, J. *Molecular Nanomagnets*, Oxford University Press, Oxford, 2006. (b) Woodruff, D. N.; Winpenny, R. E. P.; Layfield, R. A. Lanthanide Single-Molecule Magnets. *Chem. Rev.* **2013**, *113*, 5110–5148.

(2) (a) Rinehart, J. D.; Fang, M.; Evans, W. J.; Long, J. R. Strong Exchange and Magnetic Blocking in N_2^{3-} Radical-Bridged Lanthanide Complexes. *Nat. Chem.* **2011**, *3*, 538–542. (b) Rinehart, J. D.; Fang, M.; Evans, W. J.; Long, J. R. A N_2^{3-} Radical-Bridged Terbium Complex Exhibiting Magnetic Hysteresis at 14 K. *J. Am. Chem. Soc.* **2011**, *133*, 14236–14239.

(3) Demir, S.; Gonzalez, M. I.; Darago, L. E.; Evans, W. J.; Long, J. R. Giant Coercivity and High Magnetic Blocking Temperatures for N_2^{3-} Radical-Bridged Dilanthanide Complexes Upon Ligand Dissociation. *Nat. Commun.* **2017**, *8*, 2144.

(4) (a) Langley, S. K.; Wielechowski, D. P.; Vieru, V.; Chilton, N. F.; Moubaraki, B.; Abrahams, B. F.; Chibotaru, L. F.; Murray, K. S. A $\{Cr^{III}_2Dy^{III}_2\}$ Single-Molecule Magnet: Enhancing the Blocking Temperature through 3d Magnetic Exchange. *Angew. Chem. Int. Ed.* **2013**, *52*, 12014–12019. (b) Ungur, L.; Thewissen, M.; Costes, J.-P.; Wernsdorfer, W.; Chibotaru, L. F. Interplay of Strongly Anisotropic Metal Ions in Magnetic Blocking of Complexes. *Inorg. Chem.* **2013**, *52*, 6328–6337. (c) Liu, F.; Krylov, D. S.; Spree, L.; Avdoshenko, S. M.; Samoylova, N. A.; Rosenkranz, M.; Kostanyan, A.; Greber, T.; Wolter, A. U. B.; Büchner, B.; Popv, A. A. Single Molecule Magnet with an Unpaired Electron Trapped Between Two Lanthanide Ions Inside a Fullerene. *Nat. Commun.* **2017**, *8*, 16098. (d) Liu, F.; Velkos, G.; Krylov, D. S.; Spree, L.; Zalibera, M.; Ray, R.; Samoylova, N. A.; Chen, C.-H.; Rosenkranz, M.; Schiemenz, S.; et al. Air-Stable Redox-Active Nanomagnets with Lanthanide Spins Radical-Bridged by a Metal-Metal Bond. *Nat. Commun.* **2019**, *10*, 571. (e) Gould, C. A.; Mu, E.; Vieru, V.; Darago, L. E., Chakarawet, K.; Gonzalez, M. I.; Demir, S.; Long, J. R. *J. Am. Chem. Soc.* **2020**, *142*, 21197–21209.

(5) (a) Guo, F.-S.; Day, B. M.; Chen, Y.-C.; Tong, M.-L.; Mansikkamäki, A.; Layfield, R. A. A Dysprosium Metallocene Single-Molecule Magnet Functioning at the Axial Limit. *Angew. Chem. Int. Ed.* **2017**, *56*, 11445–11449. (b) Goodwin, C. A. P.; Ortu, F.; Reta, D.; Chilton, N. F.; Mills, D. P. Molecular Magnetic Hysteresis at 60 Kelvin in Dysprosocenium. *Nature* **2017**, *548*, 439–442. (c) Randall McClain, K.; Gould, C. A.; Chakarawet, K.; Teat, S. J.; Groshens, T. J.; Long, J. R.; Harvey, B. G. High-Temperature Magnetic Blocking and Magneto-Structural Correlations in a Series of Dysprosium(III) Metallocenium Single-Molecule Magnets. *Chem. Sci.* **2018**, *9*, 8492–8503. (d) Guo, F.-S.; Day, B. M.; Chen, Y.-C.; Tong, M.-L.; Mansikkamäki, A.; Layfield, R. A. Magnetic Hysteresis Up to 80 Kelvin in a Dysprosium Metallocene Single-Molecule Magnet. *Science* **2018**, *362*, 1400–1403.

(6) Rosado Piquer, L.; Sañudo, E. C. Heterometallic 3d–4f Single-Molecule Magnets. *Dalton Trans.* **2015**, *44*, 8771–8780.

(7) (a) Visinescu, D.; Desplanches, C. D.; Imaz, I.; Bahers, V.; Pradhan, R.; Villamena, F. A.; Guionneau, P.; Sutter, J.-P. Evidence for Increased Exchange Interactions with 5d Compared to 4d Metal Ions. Experimental and Theoretical Insights into the Ferromagnetic Interactions of a Series of Trinuclear $[\{M(CN)_8\}^{3-}/Ni^{II}]$ Compounds (M = Mo^V or W^V). *J. Am. Chem. Soc.* **2006**, *128*, 10202–10212. (b) Wang, X.-Y.; Avendano, C.; Dunbar, K. R. Molecular Magnetic Materials Based on 4d and 5d Transition Metals. *Chem. Soc. Rev.* **2011**, *40*, 3213–3238 and references therein.

(8) Cyano-bridged lanthanide-transition metal compounds: (a) Hozumi, T.; Ohkoshi, S.-I.; Arimoto, Y.; Seino, H.; Mizobe, Y.; Hashimoto, K. Cooling-rate Dependent Ferromagnetism in a Two-dimensional Cyano-bridged Sm(III)-W(V) Complex. *J. Phys. Chem. B* **2003**, *107*, 11571–11574. (b) Ikeda, S.; Hozumi, T.; Hashimoto, K.; Ohkoshi, S.-I. Cyano-Bridged Gadolinium(III)-Tungstate(V) Bimetallic Assembly with a One-Dimensional Chain Structure. *Dalton Trans.* **2005**, *378*, 2120–2123. (c) Przychodzeń, P.; Lewiński, K.; Pełka, R.; Bałanda, M.; Tomala, K.; Sieklucka, B. $[Ln(terpy)]^{3+}$ (Ln = Sm, Gd) Entity Forms Isolated Magnetic Chains with $[W(CN)_8]^{3-}$. *Dalton Trans.* **2006**, 625–628. (d) Tanase, S.; de Jongh, L. J.; Prins, F.; Evangelisti, M. Ferrimagnetic Heisenberg Chains Derived From $[M(CN)_8]^{3-}$ (M=Mo^V, W^V) Building-Blocks. *ChemPhysChem* **2008**, *9*, 1975–1978. (e) Prins, F.; Pasca, E.; de Jongh, L. J.; Kooijman, H.; Spek, A. L.; Tanase, S. Long-Range Magnetic Ordering in a Tb^{III}–Mo^V Cyanido-Bridged Quasi-One-Dimensional Complex. *Angew. Chem. Int. Ed.* **2007**, *46*, 6081–6084. (f) Przychodzeń, P.; Pełka, R.; Lewiński, K.; Supel, J.; Rams, M.; Tomala, K.; Sieklucka, B. Tuning of Magnetic Properties of Polynuclear Lanthanide(III)–Octacyanotungstate(V) Systems: Determination of Ligand-Field Parameters and Exchange Interaction. *Inorg. Chem.* **2007**, *46*, 8924–8938. (g) Chelebaeva, E.; Larionova, J.; Guari, Y.; Sá Ferreira, R. A.; Carlos, L. D.; Almeida Paz, F. A.; Trifonov, A.; Guérin, C. A Luminescent and Magnetic Cyano-Bridged Tb^{3+}–Mo^{5+} Coordination Polymer: Toward Multifunctional Materials. *Inorg. Chem.* **2008**, *47*, 775–777. (h) Chelebaeva, E.; Larionova, J.; Guari, Y.; Ferreira, R. A. S.; Carlos, L. D.; Paz, F. A. A.; Trifonov, A.; Guérin, C. Luminescent and Magnetic Cyano-Bridged Coordination Polymers Containing 4d–4f Ions: Toward Multifunctional Materials. *Inorg. Chem.* **2009**, *48*, 5983–5995. (i) Dhers, S.; Sahoo, S.; Costes, J.-P.; Duhayon, C.; Ramasesha, S.; Sutter, J.-P. 1-D Hydrogen-Bonded Organization of Hexanuclear {3d-4f-5d} Complexes: Evidence for Slow Relaxation of the Magnetization for $[\{L^{Me2}Ni(H_2O)Ln(H_2O)_{4.5}\}_2\{W(CN)_8\}_2]$ with Ln = Tb and Dy. *CrystEngComm* **2009**, *11*, 2078–2083. (j) Visinescu, D.; Madalan, A. M.; Andruh, M.; Duhayon, C.; Sutter, J.-P.; Ungur, L.; Van den Heuvel, W.; Chibotaru, L. F. First Heterotrimetallic {3 d-4 d-4 f} Single Chain Magnet, Constructed from Anisotropic High-Spin Heterometallic Nodes and Paramagnetic Spacers. *Chem. Eur. J.* **2009**, *15*, 11808–11814. (k) Zhou, H.; Chen, Q.; Zhou, H.-B.; Yang, X.-Z.; Song, Y.; Yuan, A.-H. Structural Conversion and Magnetic Studies of Low-Dimensional $Ln^{III}/Mo^{V}/^{IV}(CN)_8$ (Ln = Gd–Lu) Systems: From Helical Chain to Trinuclear Cluster. *Cryst. Growth Des.* **2016**, *16*, 1708–1716. (l) Alexandru, M.-G.; Visinescu, D.; Shova, S.; Lloret, F.; Julve, M. Cyanido-Bridged $\{Ln^{III}W^V\}$ Heterobinuclear Complexes: Synthesis and Magneto-Structural Study. *Inorg. Chem.* **2017**, *56*, 12594–12605. (m) Note: Trimetallic complexes in which a 3d transition metal ion is between the 4d/5d and 4f centers are not included here, since in these complexes there is typically no reasonable 4d/5d-4f magnetic coupling pathway.

(9) Non-cyanide Ln-TM bridges: (a) Pointillart, F.; Bernot, K.; Sessoli, R.; Gatteschi, D. Field Induced 4f5d $[Re(Salen)]_2O_3[Dy(Hfac)_3(H_2O)]_2$ Single Molecule Magnet. *Inorg. Chem.* **2010**, *49*, 4355–4361. (b) Martínez-Lillo, J.; Cañadillas-Delgado, L.; Cano, J.; Lloret, F.; Julve, M.; Faus, J. A. A Heteropentanuclear Oxalato-Bridged $[Re^{IV}4Gd^{III}]$ complex: Synthesis, Crystal Structure and Magnetic Properties. *Chem. Commun.* **2012**, *48*, 9242–9244. (c) Norel, L.; Feng, M.; Bernot, K.; Roisnel, T.; Guizouarn, T.; Costuas, K.; Rigaut, S. Redox Modulation of Magnetic Slow Relaxation in a 4f-Based Single-Molecule Magnet with a 4d Carbon-Rich Ligand. *Inorg. Chem.* **2014**, *53*, 2361–2363. (d) Langley, S. K.; Wielechowski, D. P.; Vieru, V.; Chilton, N. F.; Moubaraki, B.; Chibotaru, L. F.; Murray, K. S. The First 4d/4f Single-Molecule Magnet Containing a $\{Ru^{III}_2Dy^{III}_2\}$ Core. *Chem. Commun.* **2015**, *51*, 2044–2047. (e) Marinescu, G.; Maxim, C.; Clérac, R.; Andruh, M. $[Ru^{III}(valen)(CN)_2]^-$: a New Building Block To Design 4d–4f Heterometallic Complexes. *Inorg. Chem.* **2015**, *54*, 5621–5623. (f) Pejo, C.; Guedes, G. P.; Novak, M. A.; Speziali, N. L.; Chiozzone, R.; Julve, M.; Lloret, F.; Vaz, M. G. F.; González, R. Synthesis, Crystal Structure and Magnetic Properties of a Novel Heterobimetallic Rhenium(IV)–Dysprosium(III) Chain. *Chem. Eur. J.* **2015**, *21*,

8696–8700. (g) Burns, C. P.; Yang, X.; Wofford, J. D.; Bhuvanesh, N. S.; Hall, M. B.; Nippe, M. Structure and Magnetization Dynamics of Dy–Fe and Dy–Ru Bonded Complexes. *Angew. Chem. Int. Ed.* **2018**, *57*, 8144–8148. (h) Risica, G. M.; Vieru, V.; Wilkins, B. O.; Latendresse, T. P.; Reibenspies, J. H.; Bhuvanesh, N. S.; Wylie, G. P.; Chibotaru, L. F.; Nippe, M. Axial Elongation of Mononuclear Lanthanide Metallocenophanes: Magnetic Properties of Dysprosium- and Terbium-[1]Ruthenocenophane Complexes. *Angew. Chem. Int. Ed.* **2020**, *64*, 577–577.

(10)(a) Herrmann, W. A. *Synthetic Methods of Organometallic and Inorganic Chemistry*, Thieme: Stuttgart, 1997, Vol. 8. (b) Meyer, G.; Ax, P. An Analysis of the Ammonium Chloride Route to Anhydrous Rare-Earth Metal Chlorides. *Mat. Res. Bull.* **1982**, 17, 1447–1455.

(11) Evans, W. J.; Kozimor, S. A.; Ziller, J. W.; Kaltsoyannis, N. Structure, Reactivity, and Density Functional Theory Analysis of the Six-Electron Reductant, $[(C_5Me_5)_2U]_2(\mu\text{-}\eta^6\text{:}\eta^6\text{-}C_6H_6)$, Synthesized via a New Mode of $(C_5Me_5)_3M$ Reactivity. *J. Am. Chem. Soc.* **2004**, *126*, 14533–14547.

(12) Evans, W. J.; Kozimor, S. A.; Brady, J. C.; Davis, B. L.; Nyce, G. W.; Seibel, C. a.; Ziller, J. W.; Doedens, R. J. Metallocene Allyl Reactivity in the Presence of Alkenes Tethered to Cyclopentadienyl Ligands. *Organometallics* **2005**, *24*, 2269–2278.

(13) (a) Izod, K.; Liddle, S. T.; Clegg, W. A Convenient Route to Lanthanide Triiodide THF Solvates. Crystal Structures of $LnI_3(THF)_4$ [Ln = Pr] and $LnI_3(THF)_{3.5}$ [Ln = Nd, Gd, Y]. *Inorg. Chem.* **2004**, *43*, 214–218. (b) Evans, W. J.; Davis, B. L.; Champagne, T. M.; Ziller, J. W. C–H Bond Activation through Steric Crowding of Normally Inert Ligands in the Sterically Crowded Gadolinium and Yttrium $(C_5Me_5)_3M$ Complexes. *Proc. Natl. Acad. Sci. U. S. A.* **2006**, *103*, 12678–12683.

(14) Lang, J.-P.; Kawaguchi, H.; Tatsumi, K. Reactions of Tetrathiotungstate and Tetrathiomolybdate with Substituted Haloalkanes. *J. Chem. Soc. Dalt. Trans.* **2002**, 2573–2580.

(15) (a) Müller, A.; Dartmaan, M.; Römer, C.; Clegg, W.; Sheldrick, G. M. $(Ph_4P)_2[CuCN(MoS_4)]$ and $(Me_4N)_2(CuCN)_2MoS_4$: Thiomolybdate Ligands on the Cu Atoms of a CuCN Molecule and a *zigzag*-CuCN Chain. *Angew. Chem. Int. Ed.* **1981**, *20*, 1060–1061. (b) Gheller, S. F.; Hambley, T. W.; Rodgers, J. R.; Brownlee, R. T. C.; O'Connor, M. J.; Snow, M. R.; Wedd, A. G. Synthesis and Characterization of Complexes of Thiomolybdates and Thiotungstates with Copper(I) and Silver(I) Cyanides, Including ^{95}Mo and ^{183}W NMR Properties and the Crystal and Molecular Structures of $(n\text{-}Pr_4N)_2[(CN)CuS_2MoS_2]$, $(n\text{-}Pr_4N)_2[(CN)AgS_2WS_2]$, and $(Ph_4As)_2[(CN)CuS_2MoS_2Cu(CN)]\bullet H_2O$. *Inorg. Chem.* **1984**, *23*, 2519–2528. (c) Beheshti, A.; Clegg, W.; Sadr, M. H. Synthesis, Characterization and Crystal Structure Determination of $(NEt_4)_2[MS_4(CuBp')_2]\bullet X$ (M=Mo, X=$(CH_3)_2CO$; M=W, X=CH_3CN); Bp'=$H_2B(3,5\text{-}Me2Pz)_2$. *Inor. Chim. Acta* **2002**, *335*, 21–26. (d) Niu, Y.-Y.; Chen, T.-N.; Liu, S.-X.; Song, Y.-L.; Wang, Y.-X.; Xue, Z.-L.; Xin, X.-Q. Reactivity of the $[MoS_4Cu_6Br_8]^{4-}$ Anion Toward Polyarylphosphorus Ligands: Synthesis, Characterization and Nonlinear Optical Properties of $[MoS_4(Cudppf)_2]\bullet 2DMF\cdot CH_3CN$ and $[MoS_4Cu_2(Ph_2PPy)_4]$. *J. Chem. Soc. Dalt. Trans.* **2002**, 1980–1984. (e) Zheng, H.-G.; Zhou, H.-L.; Tan, W.-L.; Niu, Y.-Y.; Ji, W.; Xin, X.-Q. Solid-State Syntheses of M–Cu–S (M = Mo and W) Clusters, Crystal Structure and Non-Linear Optical Properties of $\{MS_4[Cu(p\text{-}MeOC_6H_4)_3P]_2\}\bullet 0.5C_6H_{12}$. *Inorg. Chim. Acta* **2002**, *340*, 29–34.

(16) (a) Coucouvanis, D.; Baenziger, N. C.; Simhon, E. D.; Stremple, P.; Swensen, D.; Simopoulos, A.; Kostikas, A.; Petrouleas, V.; Papaefthymiou, V. Synthesis and Structural Characterization of the $(Ph_4P)_2[Cl_2FeS_2MS_2FeCl_2]$ Complexes (M = Mo, W). First Example of a Doubly Bridging Thiomolybdate (MoS_4) Unit and its Possible Relevance as a Structural Feature in the Nitrogenase Active Site. *J. Am. Chem. Soc.* **1980**, *102*, 1732–1734. (b) Müller, A.; Jostes, R.; Schmitz, K.; Krickemeyer, E.; Bögge, H.; Bill, E.; Trautwein, A. $(PPh_4)_2[Cl_2Fe(ReS_4)FeCl_2]_{0.7}[Cl_2Fe(MoS_4)FeCl_2]_{0.3}$: Containing Two Isostructural Complexes with Different Electronic Populations, Mössbauer Spectra and Electronic Structures. *Inorg. Chim. Acta* **1988**, *149*, 9–12. (c) Müller, A.; Krickemeyer, E.; Bögge, H. Entry into the Chemistry of Simple Rhenium-Sulfur Complexes and Clusters. Representation and Crystal Structure of $R[ReS_4]$, $R'[ReS_9]$, $(NH_4)_4[Re_4S_{22}]\bullet 2H_2O$, $R'_2[Cl_2Fe(MoS_4)FeCl_2]_x[Cl_2Fe(ReS_4)FeCl_2]_{1-x}$, $R'_2[(ReS_4)Cu_3I_4]$ and $RR'_2[(ReS_4)Cu_5Br_7]$ (R = NEt_4; R' = PPh_4; x = 0.3, 0.5). *Z. Anorg. Allg. Chem.* **1987**, *554*, 61–78.

(17) Blacque, O.; Brunner, H.; Kubicki, M. M.; Lucas, D.; Meier, W.; Mugnier, Y.; Nuber, B.; Stubenhofer, B.; Wachter, J. Syntheses and Properties of Tetrathio- and Tetraseleno Metalates $[(C_5Me_4R)_2NbE_2]_2M$ (E=S, Se; M=Cr, Mo; R=Me, Et) with Peripheric Niobocene Ligands. *J. Organomet. Chem.* **1998**, *564*, 71–79.

(18) Evans, W. J.; Ansari, M. A.; Ziller, J. W.; Khan, S. I. Organosamarium Tetrathiometalate Chemistry: Synthesis and Structure of the Mixed-Metal Complexes $\{[(C_5Me_5)_2Sm]_2Mo(\mu\text{-}S)_4\}^-$ and $\{[(C_5Me_5)_2Sm]_2(\mu\text{-}S)_2WS_2\}^-$. *Organometallics* **1995**, *14*, 3–4.

(19) Connelly, N. G.; Geiger, W. E. Chemical Redox Agents for Organometallic Chemistry. *Chem. Rev.* **1996**, *96*, 877–910.

(20) Stoll, S.; Schweiger, A. EasySpin, A Comprehensive Software Package for Spectral Simulation and Analysis in EPR. *J. Magn. Reson.* **2006**, *178*, 42–55.

(21) (a) Greenblatt, M.; Strobel, P.; Pifer, J. H. Magnetic resonance study of Mo^{5+} in $Ca_{1-x}Y_xMoO_4$. *J. Chem. Phys.* **1981**, *74*, 6580–6583. (b) Pifer, J. H.; Ziemski, S.; Greenblatt, M.; Wanklyn, B. M. ESR of Mo^{5+} in YVO_4: A Substitutional Off-Center Ion. *J. Solid State Chem.* **1982**, *45*, 93–98. (c) Schäfer, R.; Fiedler, J.; Moscherosch, M.; Kaim, W. First Characterization of a Tetrathiomolybdate(V) Derivative by EPR, UV–VIS and IR Spectroelectrochemistry. *J. Chem. Soc. Chem. Commun.* **1993**, *114*, 896–897. (d) Ecclestone, T.; Laurie, S. H.; Symons, M. C. R.; Taiwo, F. A. EPR Studies on Irradiated Group VI Tetrachalconide Ions. *Polyhedron* **1998**, *17*, 1435–1438.

(22) Greenblatt, M.; Pifer, J. H.; McGarvey, B. R.; Wanklyn, B. M. Electron Spin Resonance of Cr^{5+} in YPO_4 and YVO_4. *Chem. Phys.* **1981**, *74*, 6014–6017.

(23) MacDonald, M. R.; Bates, J. E.; Ziller, J. W.; Furche, F.; Evans, W. J. Completing the Series of +2 Ions for the Lanthanide Elements: Synthesis of Molecular Complexes of Pr^{2+}, Gd^{2+}, Tb^{2+}, and Lu^{2+}. *J. Am. Chem. Soc.* **2013**, *135*, 9857–9868.

(24) (a) Abragam, A.; Bleaney, B. *Electron Paramagnetic Resonace of Transtion Ions*, Clarendon Press: Oxford, 1970. (b) McGarvey, B. R. In *Transition Metal Chemistry, a Series of Advances*; Carlin, R. L., Ed.; Marcel Dekker: New York, 1966.

(25) Záliš, S.; Stoll, H.; Baerends, E. J.; Kaim, W. The d^0, d^1 and d^2 Configurations in Known and Unknown Tetrathiometal Compounds MS_4^{n-} (M = Mo, Tc, Ru; W, Re, Os). A Quantum Chemical Study. *Inorg. Chem.* **1999**, *38*, 6101–6105.

(26) (a) Balasubramani, S. G. et al. TURBOMOLE: Modular program suite for ab initio quantum-chemical and condensed-matter simulations. *J. Chem. Phys.* **2020**, *122*, 184107. (b) Staroverov, V. N.; Scuseria, G. E.; Tao, J.; Perdew, J. P. Comparative Assessment of a New Nonempirical Density Functional: Molecules and Hydrogen-Bonded Complexes. *J. Chem. Phys.* **2003**, *119*, 12129–12137.

(27) (a) Kober, E. M.; Meyer, T. J. Concerning the Absorption Spectra of the Ions $M(Bpy)_3^{2+}$ (M = Fe, Ru, Os; Bpy = 2,2'-Bipyridine). *Inorg. Chem.* **1982**, *21*, 3967–3977. (b) Schäfer, R.; Kaim, W.; Moscherosch, M.; Krejčik, M. Tetrathiorhenate(VI), ReS_4^{2-}. Spectroelectrochemical Characterization (UV–VIS–IR) of a Small New d^1 System and of Its Tetrakis(2,2'-bipyridine)diruthenium(II) Complex (EPR). *J. Chem. Soc., Chem. Commun.* **1992**, *93*, 834–835.

(28) (a) Sabbatini, N.; Bonazzi, A.; Ciano, M.; Balzani, V. Electron-Transfer Quenching and Outer-Sphere Charge-Transfer Transitions in Mixed-Metal Ion Pairs. the $[Eu\subset 2.2.1]^{3+}$-$M(CN)_6^{4-}$ Systems. *J. Am. Chem. Soc.* **1984**, *106*, 4055–4056. (b) Chorazy, S.; Arczynski, M.; Nakabayashi, K.; Sieklucka, B.; Ohkoshi, S.-I. Visible to Near-Infrared Emission From Ln^{III}(Bis-Oxazoline)–$[Mo^{V}(CN)_8]$ (Ln = Ce–Yb) Magnetic Coordination Polymers Showing Unusual Lanthanide-Dependent Sliding of Cyanido-Bridged Layers. *Inorg. Chem.* **2015**, *54*, 4724–4736. (c) Yoshida, T.; Cosquer, G.; Izuogu, D. C.; Ohtsu, H.; Kawano, M.; Lan, Y.; Wernsdorfer, W.; Nojiri, H.; Breedlove, B. K.; Yamashita, M. Field-Induced Slow Magnetic Relaxation of Gd^{III} Complex with a Pt–Gd Heterometallic Bond. *Chem. Eur. J.* **2017**, *125*, 3576–3577. (d) Yoshida, T.; Izougu, D. C.; Iwasawa, D.; Ogata, S.; Hasegawa, M.; Breedlove, B. K.; Cosquer, G.; Wernsdorfer, W.; Yamashita, M. Multiple Magnetic Relaxation Pathways and Dual-Emission Modulated by a Heterometallic Tb-Pt Bonding Environment. *Chem. Eur. J.* **2017**, *23*, 10527–10531.

(29) Chilton, N. F.; Anderson, R. P.; Turner, L. D.; Soncini, A.; Murray, K. S. PHI: A Powerful New Program for the Analysis of Anisotropic Monomeric and Exchange-Coupled Polynuclear d- and f-Block Complexes. J. Comput. *Chem.* **2013**, *34*, 1164–1175.

(30) Hu, Z.; Dong, B.-W.; Liu, Z.; Liu, J.-J.; Su, J.; Yu, C.; Xiong, J.; Shi, D.-E.; Wang, Y.; Wang, B.-W.; Ardavan, A.; Shi, Z.; Jiang, S.–D.; Gao, S. Endohedral Metallofullerene as Molecular High Spin Qubit: Diverse Rabi Cycles in $Gd_2@C_{79}N$. *J. Am. Chem. Soc.* **2018**, *140*, 1123–1130.

(31) Meihaus, K. R.; Corbey, J. F.; Fang, M.; Ziller, J. W.; Long, J. R.; Evans, W. J. Influence of an Inner-Sphere K+ Ion on the Magnetic Behavior of N_2^{3-} Radical-Bridged Dilanthanide Complexes Isolated Using an External Magnetic Field. *Inorg. Chem.* **2014**, *53*, 3099–3107.

(32) Costes, J.-P.; Dahan, F. O.; Dupuis, A. Influence of Anionic Ligands (X) on the Nature and Magnetic Properties of Dinuclear $LCuGdX_3{\cdot}nH_2O$ Complexes (LH_2 Standing for Tetradentate Schiff Base Ligands Deriving from 2-Hydroxy-3-methoxybenzaldehyde and X Being Cl, N_3C_2, and CF_3COO). *Inorg. Chem.* **2000**, *39*, 165–168.

(33) Müller, A.; Diemann, E.; Jostes, R.; Bögge, H. Transition Metal Thiometalates: Properties and Their Significance in Complex and Bioinorganic Chemistry. *Angew. Chem. Int. Ed.* **1981**, *20*, 934–955.

(34) Kollmar, C.; Kahn, O. Ferromagnetic Spin Alignment in Molecular Systems: An Orbital Approach. *Acc. Chem. Res.* **1993**, *26*, 259–265.

(35) Guo, Y.-N.; Xu, G.-F.; Wernsdorfer, W.; Ungur, L.; Guo, Y.; Tang, J.; Zhang, H.-J.; Chibotaru, L. F.; Powell, A. K. Strong Axiality and Ising Exchange Interaction Suppress Zero-Field Tunneling of Magnetization of an Asymmetric Dy_2 Single-Molecule Magnet. *J. Am. Chem. Soc.* **2011**, *133*, 11948–11951.

(36) Tuna, F.; Smith, C. A.; Bodensteiner, M.; Ungur, L.; Chibotaru, L. F.; McInnes, E. J. L.; Winpenny, R. E. P.; Collison, D.; Layfield, R. A. A High Anisotropy Barrier in a Sulfur-Bridged Organodysprosium Single-Molecule Magnet. *Angew. Chem. Int. Ed.* **2012**, *51*, 6976–6980.

(37) Demir, S.; Zadrozny, J. M.; Long, J. R. Large Spin-Relaxation Barriers for the Low-Symmetry Organolanthanide Complexes $[Cp^*_2Ln(BPh_4)]$ (Cp^* = pentamethylcyclopentadienyl; Ln = Tb, Dy). *Chem. Eur. J.* **2014**, *20*, 9524–9529.

(38) Barra, A. L.; Caneschi, A.; Cornia, A.; Gatteschi, D.; Gorini, L.; Heiniger, L.-P.; Sessoli, R.; Sorace, L. The Origin of Transverse Anisotropy in Axially Symmetric Single Molecule Magnets. *J. Am. Chem. Soc.* **2007**, *129*, 10754–10762.

(39) Benelli, C.; Gatteschi, D. Magnetism of Lanthanides in Molecular Materials with Transition-Metal Ions and Organic Radicals. *Chem. Rev.* **2002**, *102*, 2369–2388.

TOC Graphic:

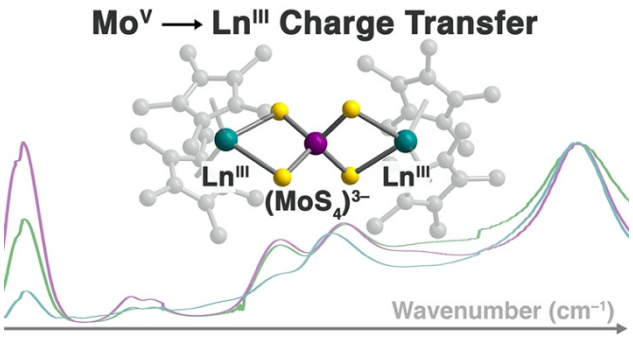
Mo^{V} ⟶ Ln^{III} Charge Transfer
Ln^{III}
Ln^{III}
(MoS$_4$)$^{3-}$
Wavenumber (cm^{-1})